β-Lactoglobulin–carboxymethylcellulose core–shell microparticles: Construction, characterization and isolation

L. Carpineti [a], María J. Martinez [a,b], Ana M.R. Pilosof [a,b], Oscar E. Pérez [a,b,*]

[a] Departamento de Industrias, Facultad de Ciencias Exactas y Naturales, Universidad de Buenos Aires, Ciudad Universitaria, 1428 Buenos Aires, Argentina
[b] Consejo Nacional de Investigación Científica y Técnicas de la República Argentina (CONICET), Argentina

ABSTRACT

The aim of this work was to build, to isolate and to characterize, core–shell microparticles composed of a core of thermally aggregated β-lactoglobulin (β-lg) covered by a shell of carboxymethylcellulose (CMC). The core–shell particles were obtained by mixing $(\beta\text{-lg})_n$ and CMC solutions at pH 7 and finally, decreasing the pH up to 4, promoting the adsorption of CMC on the protein core due their opposite electric charge. The core–shell microparticles were characterized by static laser light scattering (SLS), optical microscopy and atomic force microscopy (AFM). At pH 4, $(\beta\text{-lg})_n$ showed a diameter ∼200 nm, but after adding the polysaccharide had a diameter ∼1 μm. The microscopy corroborated the data obtained by SLS measurements. Core–shell microparticles could be isolated by lyophilization and potentially applied as a fat replacement and/or a delivery systems for encapsulated substances in food formulations.

© 2014 Elsevier Ltd. All rights reserved.

1. Introduction

Into the food science and technology field, the definition for core–shell structures includes particulate systems made from biocompatible polymers, as proteins and polysaccharides or lipids. The core is formed by one of them and the shell, surrounding the core, is composed by other chemical specie. Particles with core–shell structures have been used to ensure materials with at least two kinds of properties, i.e., one endowed by the core and the other by the shell (Mandal et al., 2013). The core–shell systems have a great number of applications, in the pharmaceutical industry and in the nutraceutical development. They can be used for encapsulating, protecting and for exerting a controlled delivery of bioactive components as minerals, peptides, proteins, enzymes, drugs, lipids or dietary fibers (Chen et al., 2006; Elzoghby et al., 2011; Emerich and Thanos, 2007; Goldberg et al., 2007; Kulkarni et al., 2005; Ubbink and Kruger, 2006). Core–shell particles that can mimic the lipids drops in foods deserve a special mention, because of their properties for light dispersion, enhance viscosity and to give the fat sensation into the mouth. Thus, this particles find a new application as fat substituent (Santipanichwong et al., 2008).

One way to achieve the core–shell microparticles construction can be by mixing proteins aggregates previously formed and polysaccharides solutions at pH and ionic strength in which both species have opposite electrostatic net charge between the molecules (Turgeon et al., 2003). As such an association can be reversible when the solution pH or ionic strength are changed (Coviello et al., 2007; Lakkis and Thies, 2007), this kind of particles should have a well defined range of the medium conditions for the structural integrity maintenance.

For the core–shell structures, several proteins have been used, for instance caseins (Dalgleish, 1990), and globular proteins as those derived from whey, egg and soy, which are capable to self-associate under conditions where protein–protein interactions are favoured (Akkerman et al., 2007; Broersen et al., 2006) and the result is the aggregate formation. The size and the concentration of these particles can be controlled by pH, ionic strength, temperature, stirring time, etc. Among the polysaccharides, modified starch, alginate, dextran, cellulose derivatives and hyaluronic acid were mainly used for the core–shell microparticle construction (Ilgin et al., 2011; Laville et al., 2013; Mirabedini et al., 2012; Murúa-Pagola et al., 2009; Wu et al., 2013).

Carboxymethylcellulose (CMC) is an anionic cellulose derivative with carboxymethyl groups bound to the hydroxyl groups of the glucose unit. CMC being water soluble (Su et al., 2010) is the more important cellulose derivative for the industry (Heinze and Liebert, 2001). Some examples of its applications in the food industry are: as a thickener because of its water binder capacity, in the oil industry as a lubricant for drilling, and in the cosmetic industry as a stabilizer and a binder, since it is non-toxicity, biodegradable and

* Corresponding author at: Departamento de Industrias, Facultad de Ciencias Exactas y Naturales, Universidad de Buenos Aires, Ciudad Universitaria, 1428 Buenos Aires, Argentina. Tel.: +54 11 45763377; fax: +54 11 45763366.
E-mail address: operez@di.fcen.uba.ar (O.E. Pérez).

biocompatible (Lee et al., 2009). It posses good barrier properties, it is non-toxic and a relatively low price (Vásconez et al., 2009).

Bovine β-lactoglobulin (β-lg) is a globular whey protein member of the lipocalin family with a molar mass about 18.4 kDa and a diameter of 4 nm (Aymard et al., 1999). This protein has been studied extensively with a wide range of techniques due to a great commercial importance to the food industry. At temperatures higher than 60 °C the protein denatures and aggregates irreversibly. This aggregation is dependent on pH. The isoelectric point of β-lg is around 4.8–5.2 (Harnsilawat et al., 2006), so the size of β-lg aggregates (β-lg)$_n$ is different at pH above and below pI (Hoffmann and van Mil, 1999; Mehalebi et al., 2008; Schokker et al., 2000, 1999; Sharma et al., 1996; Surroca et al., 2002; Verheul et al., 1998).

The approach used in the present work implied, to form firstly a core of (β-lg)$_n$ by heating the protein solutions and secondly the shell deposition by promoting the electrostatic union of the CMC molecules on the previously formed core. Then the core shell microparticles were submitted to a lyophilization process in order to isolate them. This process has been commonly used to formulate food products into solid forms to overcome the instability induced by storage conditions and expanding the materials shelf life.

Therefore the aim of this work was to obtain and characterize core shell microparticles constituted by a (β-lg)$_n$ core and a CMC shell. The potential changes induced by lyophylization and rehydration on the particles in their size and morphology were also analyzed.

2. Materials and methods

2.1. Materials

BioPURE β-lactoglobulin (β-lg) was supplied by DAVISCO Foods International, Inc. (Le Sueur, Minnesota, United States). Its composition was: protein (dry basis) 97.8% being β-lactoglobulin 93.6% of total proteins, fat 0.3%, ash 1.8% and moisture 5.0%. Carboxymethylcellulose (CMC), commercially named E466, was provided by C-DIA S.R.L. Argentina with a degree of substitution 0.75–0.95, purity 99.5% and moisture 10%. Molar mass of CMC is 17,000 Da with a degree of polymerization equal to 100 determined according to European Directive 1996/77/CE (1996) for CMC. Viscosity, measured on 1% aqueous solution of CMC, at 25 °C, was 4000 ± 400 cP as determined by Brookfield RVT viscometer (20 rpm sp 3). Coomassie Brillant Blue G250 used to stain the solutions for optical microscopy measurements was supplied by Fluka Chemika (Switzerland).

2.2. Solutions preparation

β-lg (0.25%, 0.5% and 1%) and CMC (0.005–0.6%) aqueous solutions were prepared freshly and separately by dissolving the proper amount of powder in Milli-Q ultrapure water at room temperature and gently stirring for 30 min in a magnetic stirrer IKA® C-MAG HS7 (China). After that, solutions were filtered through 0.45 and 0.22 µm microfilters (Whatman International Ldt, Maidstone, England). pH was adjusted at the required value, which oscillated between 2 and 7, with 0.1 or 1 N of NaOH or 0.1 or 1 N of HCl. To avoid bacterial growth 0.02% wt NaN$_3$ was added. Finally the solutions were kept 24 h at 4 °C to achieve the maximum protein and polysaccharide molecules hydration.

For the case of (β-lg)$_n$, construction β-lg 0.25% (wt) aqueous solutions were heated at 80 °C for 15 min at pH 7. Aggregates, very well defined in size, kept suspended in the aqueous media were obtained under such conditions (Santipanichwong et al., 2008).

After heat treatment, the samples were immediately put into a bath containing water/ice.

2.3. (β-lg)$_n$ and CMC particle size determinations

Dynamic light scattering experiments were carried out in a dynamic laser light scattering (DLS) (Zetasizer Nano-Zs, Malvern Instruments, Worcestershire, United Kingdom) with a measurements range of 0.6 nm to 6 µm, provided with a He-Ne laser (633 nm) and a digital correlator, Model ZEN3600. Measurements were carried out at a fixed scattering angle of 173°. Samples were contained in a disposable polystyrene cuvette. In DLS, the sample is illuminated with a laser beam and the intensity of the resulting scattered light produced by the particles fluctuates at a rate that is dependent upon the size of the particles. Analysis of these intensity fluctuations yields the diffusion coefficient of the particle and hence the particle size using de Stokes–Einstein equation Eq. (1) (Berne and Pecora, 1976):

$$R_H = \frac{k \cdot T}{6 \cdot \pi \cdot \eta \cdot D} \tag{1}$$

where $d(H)$ is the hydrodynamic diameter; D is translational diffusion coefficient; k is Boltzmann's constant; T is absolute temperature and η is viscosity.

To obtain size information the CONTIN approach was applied, by which the data for percentile distribution of particle/aggregate sizes is obtained. This size distribution is a plot of the relative intensity of light scattered by particles in various size classes and it is therefore known as an intensity size distribution. Through Mie theory, it is possible to convert the intensity distribution to volume distribution, which is important to analyze in order to understand the relative significance of each peak, due to the peaks of higher size generate greater intensity than the smaller ones because the intensity is proportional to the square of the molar mass (Malvern-Instruments; Navarra et al., 2007).

For DLS determinations, protein and polysaccharide solutions were previously filtered through a 0.45, 0.22 and 0.02 µm microfilter (Whatman International Ltd., England). The assay was performed in triplicate on three individual samples.

2.4. ζ-Potential measurements

ζ-Potential measurements were also performed in a dynamic laser light scattering instrument (Zetasizer Nano–Zs, Malvern Instruments, Worcestershire, United Kingdom). The ζ-potential was evaluated from the electrophoretic mobility of the particles. The conversion of the measured electrophoretic mobility data into ζ-potential was done using Henry's equation Eq. (2) (Hunter, 2001):

$$U_e = 2\varepsilon\zeta f(Ka)/3\eta \tag{2}$$

where U_e is the electrophoretic mobility, ε the dielectric constant, η the sample viscosity and $f(Ka)$ the Henry's function. The reported values are the average and standard deviation of three measurements.

To perform these determinations, previously filtered solutions were put into disposable capillary cells, (DTS1060, Malvern Instruments, Worcestershire, United Kingdom).

2.5. Core–shell microparticle construction and size determination

The core–shell microparticles were prepared by applying the electrostatic deposition concept (Jones and McClements, 2011). To this end the appropriate volume of each double concentrated (β-lg)$_n$ suspension and CMC solution, were mixed up to achieve the required final concentration. The suspension of (β-lg)$_n$ and

CMC solutions were mixed at pH 7.0; where the possibility of electrostatic interactions was reduced because of net negative charge of both biopolymers at this pH value. Then, the pH of the mixture was carefully decreased up to 4.0, promoting thus the electrostatic adsorption of the positive polysaccharide on the negative charged $(\beta\text{-lg})_n$ surface.

2.5.1. Particle size determination

Particle size distribution of core–shell microparticles was determined by static light scattering (SLS) using a Mastersizer 2000 device equipped with a Hydro 2000MU as dispersion unit, from Malvern Instruments Ltd (Worcestershire, UK). The pump speed was settled at 1300 rpm. The refractive index (RI) of the disperse phase (1.354) and its absorption parameter (0.001) were used. Particle size is reported as D_{32} and D_{43} diameters. D_{32} is the volume–surface mean diameter or Sauter diameter ($D_{32} = \Sigma n_i d_i^3 / \Sigma n_i d_i^2$) where n_i is the number of particles of diameter (Huang et al., 2001; Leroux et al., 2003). D_{43} is the equivalent volume-mean diameter or De Broucker diameter ($D_{43} = \Sigma n_i d_i^4 / \Sigma n_i d_i^3$), where n_i is the number of particles of diameter d_i (Galazka et al., 1996; Gu et al., 2005; Güzey et al., 2004; Huang et al., 2001; Leroux et al., 2003). The particle sizes are reported as the average and standard deviation of 10 readings made on two independently prepared samples.

2.5.2. Optical microscopy

Images of $(\beta\text{-lg})_n$ and core–shell microparticles were taken using an Olympus Corp. microscope model BX43 (Tokyo, Japan) equipped with a digital camera (Q-Color 3C, Canada). The following Olympus objective lenses were used: 40x y 100x, For labeling the protein molecules few drops of Coomassie Brillant Blue solution 0.02% (w/v) was added to each solution. This colorant, derived from trimethylmethane, has a big affinity with protein molecules. Digital image files were acquired in multiple.tif format in 1024 × 1024 and 512 × 512 pixel resolutions by image acquisition software (Qcapture pro® 6.0, QImaging, Canada) also from Olympus Corp.

2.5.3. AFM images

The methodology proposed by (Lavaggi et al., 2010) was followed. Briefly, 5 μL of each suspension, 1×10^{-6}% (wt), were put to a freshly cleaved mica and then adsorbed to a surface (glued to steel disks), allowed to incubate at room temperature, and adsorbed to a freshly cleaved mica surface (glued to steel disks). Then gently washed with Milli-Q water, and dried under a gentle stream of filtered, dry nitrogen. In some cases, the samples were further dried under vacuum. AFM imaging was performed on a Vecco-Digital Instruments microscope, model Multimode (MMAFM) NanoScope IIIa-Quadrex, with a vertical J scanner having a maximal lateral range of approximately 150 μm. All images that are shown were analyzed by tapping in air. Standard silicon cantilevers 125 μm in length were used for all tapping in air images. The cantilever oscillation frequency was tuned to 280–320 nm, and samples were scanned at 3–5 lines/s. Images were processed by flattening (using NanoScope software) to remove background slope. Experiments were carried out in a temperature controlled room at 20 ± 1 °C, with acoustic hood isolation and active vibration damping.

2.6. Core–shell microparticles isolation and freeze-drying effects

50 mL of the suspensions under analysis were put into Petri dishes and frozen by immersion in liquid nitrogen (−196 °C) and freeze dried in a Heto Holten A/S, cooling trap model CT 110 freeze-dryer, Heto Lab Equipment, Denmark, operating at a condenser plate temperature of −111 °C, a chamber pressure of 30 Pa, and shelf temperature of 25 °C. The secondary drying was

also performed at 25 °C. The moisture content of the samples was subtracted to the amount of water added to reach the original core–shell concentration in the rehydrated suspension. Powders moisture content was determined as indicated by the NTC 529-ISO 6731 method (1989).

In order to analyze the possible changes induced by the freeze drying process on the core shell microparticles size distribution, their integrity and morphology, the powders were rehydrated in ultrapure water, pH 4, and the procedures detailed in Sections 2.5.1–2.5.3 were followed.

3. Results and discussion

3.1. Single biopolymer characterization by size

3.1.1. $(\beta\text{-lg})_n$

$(\beta\text{-lg})_n$, which constituted the core of the core–shell microparticles, were generated under controlled conditions of temperature and time. A study of the β-lg aggregates size distribution under conditions of variable pH was performed by DLS, which allowed evaluating the particle size distribution (Fig. 1). At this respect, the intensity size distributions (Fig. 1A) showed bimodal behavior at pH 2 and 7, with maximum values at 4 nm. Populations with peaks corresponding to the highest sizes felt between 20 and 200 nm. However, the number of particle with the highest sizes was negligible as can be deduced from the volume size distribution (Fig. 1B). On the other hand, the heated β-lg solutions at pH 4 and 6,
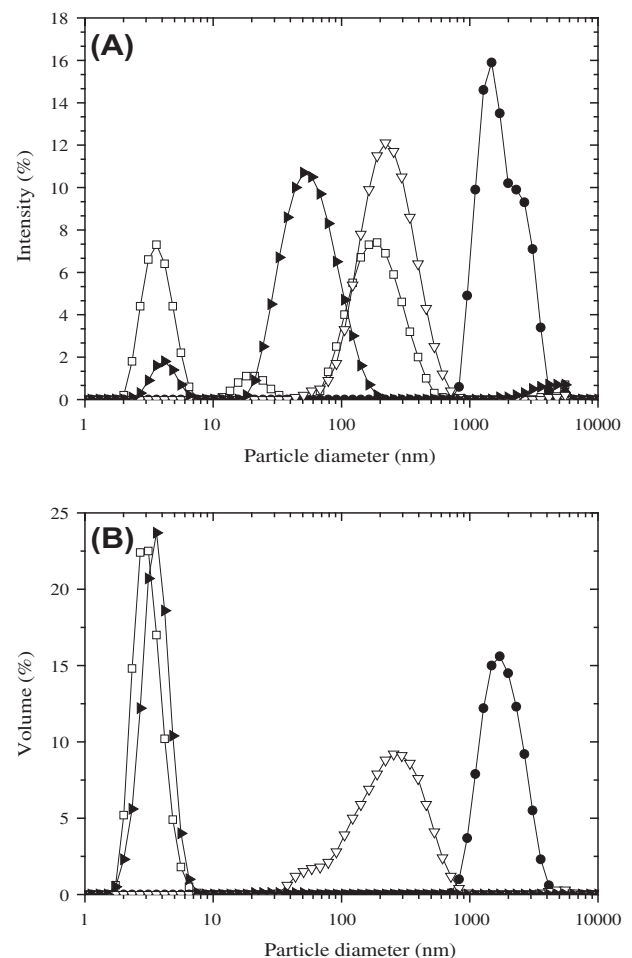

Fig. 1. Intensity (A) and volume (B) size distribution of $(\beta\text{-lg})_n$ at pH: (□) 2, (●) 4, (▽) 6 and (▶) 7. Temperature for DLS measurements 25 °C.

presented only one peak at higher sizes with maximum values at 1500 and 200 nm for pH 4 and 6, respectively, which were also present in the volume size distributions (Fig. 1B), in coincidence with other reports (Aberkane et al., 2012; Lesmes and McClements, 2012). Two reasons were decisive to choose the pH 6 for the protein solution heating: (1) The highest amount of protein monomer associated, i.e. the majority native β-lg molecules reacted forming (β-lg)$_n$, and (2) the particle size distribution expressed in volume indicated no presence of aggregates lower than 10 nm in diameter. In line with this finding, Mehalebi et al. (2008) pointed out that stable soluble aggregates were formed in a reproducible way into the pH ranged between 5.8 and 9.0.

3.1.2. CMC

Polysaccharide size distribution was also determined from 0.01% wt, solutions, at its natural pH. This concentration was chosen just for methodological reasons, since at higher concentrations the polysaccharide solutions manifested very high viscosities and the DLS measurements lose accuracy. The macroscopic aspect of the polysaccharide solution did not vary with the pH solution (not shown). On the other hand, they showed high dependence of the CMC size distribution on the pH medium (Fig. 2). Thus, at the natural pH obtained just after CMC dissolution a predominant peak in the intensity size distribution was observed (Fig. 2A) with a maximum value at 150 nm; however, when the result was analyzed by volume (Fig. 2B) two peaks are present, a predominant
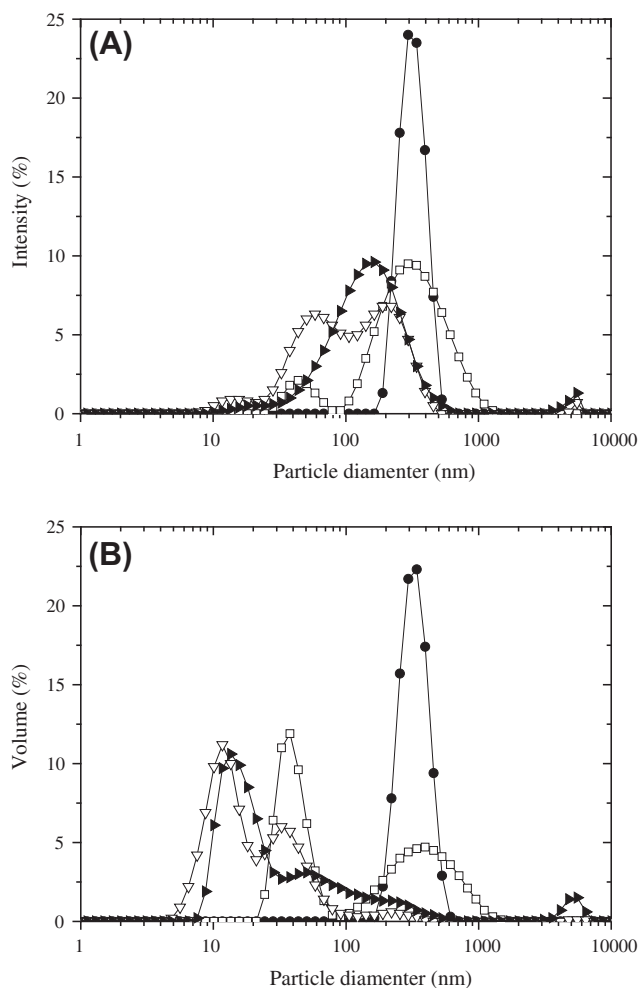
peak at 15 nm and the other with size between 40 and 300 nm. At pH 6, CMC shows a multimodal behavior in both intensity and volume size distributions. In the first plot, the main maximum values peaks were 40 and 300 nm and a little peak at 10 nm, while in volume plot predominated the peaks with the lower maximum values (at 10 and 40 nm), suggesting that the peak of 300 nm is negligible in number. The intensity and volume size distribution at pH 4 was bimodal with maximum values at 40 and 300–400 nm. And finally, at pH 2 the CMC behavior was monomodal with maximum value close to 300 nm.

3.2. Core–shell microparticles construction

In order to find the adequate pH conditions for core–shell microparticles constitution, single species previously characterized in terms of size, were analyzed comparatively in terms of surface charge. Fig. 3 shows the ζ-potential values for both, (β-lg)$_n$ and CMC aqueous solutions, as a function of pH. It can be seen that ζ-potential varied between −54.5 mV at pH 7 and 26.4 mV at pH 2 for (β-lg)$_n$, with a point of zero charge around pH 4.5. (β-lg)$_n$ behaved similarly to native β-lg solutions without heating which have a pI between 4.6 and 5.2 (Bromley et al., 2005; Harnsilawat et al., 2006; Santipanichwong et al., 2008). The electrical charge of CMC solutions ranged between 6.75 mV and −26.6 mV. The global surface charge corresponding to zero for CMC was around pH 2.25, which keep correspondence with the low pK_a values of the anionic groups (–COO$^-$) of this polysaccharide (Chanasattru et al., 2009; Hansen et al., 1971). The analysis of ζ-potential-pH curves, superimposed for both species (Fig. 3), allowed to establish the optimum pH range for the electrostatic deposition of the CMC molecules on the (β-lg)$_n$, which was between 2.25 and approximately 4.25 (gray zone in Fig. 3). Thus, pH 4.0 was selected due to practical benefits since it was more easily adjusted. As the pH was reduced, the number of cationic groups on the (β-lg)$_n$ increase which induced the electrostatic attraction with the polysaccharide anionic groups.

In practice, the electrostatic adsorption of CMC on the protein aggregates generated structures of a higher size, whose dimensions clearly fell into the so called microscale (>1 μm) (Ho et al., 2013).

3.2.1. Characterization by size

Static light scattering principle was applied for their characterization. Fig. 4 shows the results concerning to the effects of the polysaccharide concentration on the (β-lg)$_n$ particle size distribution. Several CMC bulk concentrations were assessed, only four of

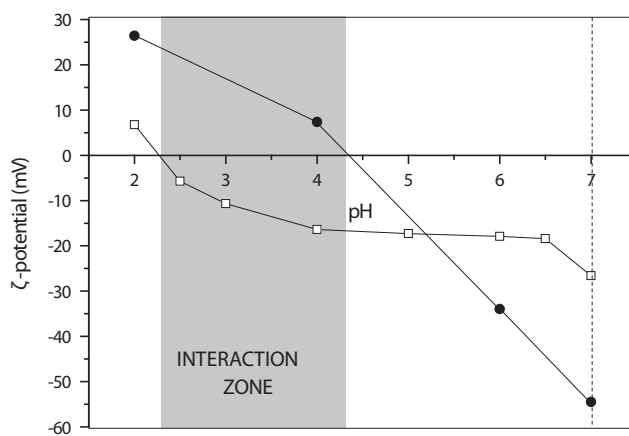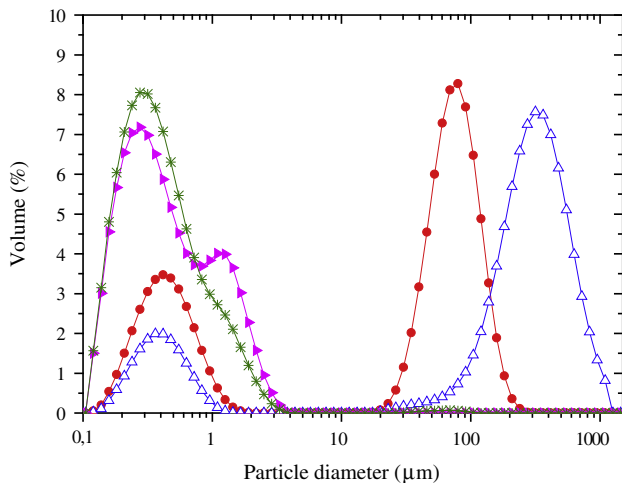**Fig. 2.** Intensity (A) and volume (B) size distribution of CMC aqueous solutions (0.01% wt) at pH: (●) 2, (□) 4, (▽) 6 and (►) 7. Temperature for DLS measurements 25 °C.

Fig. 3. Influence of pH on the electrical charge (ζ-potential) of aqueous solutions containing: (●) (β-lg)$_n$ and (□) CMC 0.01% wt. Temperature for DLS measurements 25 °C.

Fig. 4. Volume size distribution of $(\beta\text{-lg})_n$ + CMC (($\bullet$) 0.02, ($\triangle$) 0.04; ($\blacktriangleright$) 0.15; ($*$) 0.3% wt). Temperature for SLS measurements 25 °C.

of several $(\beta\text{-lg})_n$ units. At higher CMC concentration, the contribution of populations of highest sizes to the global size distribution (Fig. 4) remarkable decreased and consequently the D_{43} values also decreased. Such an effect can be explained as the decrease in the *bridging flocculation*, in analogy to the food emulsion science, at the higher CMC concentration. Briefly, the long polysaccharide chains are able to bind more than one protein aggregate, which can form clusters. In bridging flocculation the electrically charged biopolymers are capable of adsorbing to the surfaces of oppositely charged nanoparticles through electrostatic interactions and promote flocculation due to charge neutralization and bridging effects. Bridging flocculation is most pronounced at polysaccharide concentrations where the particle surfaces are only partially covered (Anarjan and Tan, 2013; Santipanichwong et al., 2008).

them are shown in the figure for the clarity sake, i.e. 0.02%; 0.04%; 0.15% and 0.3%. Two principal populations can be observed for the $(\beta\text{-lg})_n$ + CMC systems when the amount of polysaccharide was lower than 0.15%. At CMC concentrations 0.15% or higher, two effects were observed as the polysaccharide concentration increased: the size distribution tended to be monomodal and the global distribution of particle size was shifted to lower values. The increase in the polysaccharide concentration exerted such a gradual effect in the particle size distribution, that even a shoulder could be observed at 0.15% of CMC, whose peak corresponded to 1.5 µm. Thus, at the maximum polysaccharide concentration (0.3%, wt), the measured range of particle size was between 0.1 and 3 mm, no shoulder was detected. The particles size decreased remarkably after CMC adsorption at the $(\beta\text{-lg})_n$ surface.

D_{43} is a parameter related to the volume occupied by the particles and therefore it is more sensitive to the particle size changes (Arzeni et al., 2012). Table 1 shows the variation for the D_{43} diameter of the formed microstructure with variable CMC bulk concentrations. In the absence of CMC, the D_{43} diameter of $(\beta\text{-lg})_n$ showed the lowest value, which manifested an increase as the polysaccharide concentration increase. The maximum values corresponded to the mixture containing 0.04% and 0.075% (wt) of polysaccharide; these values being statistically different kept resemblance from a practical point of view. The reversibility for the D_{43} at lower values when the CMC concentration was 0.15–0.3% (wt), can be interpreted as the complete coverage of the surface protein nanoparticle by the polysaccharide as was previously pointed out by Santipanichwong et al. (2008).

Low CMC concentration provoked an increase in D_{43} diameter, i.e. the amount of the polysaccharide would induce the aggregation
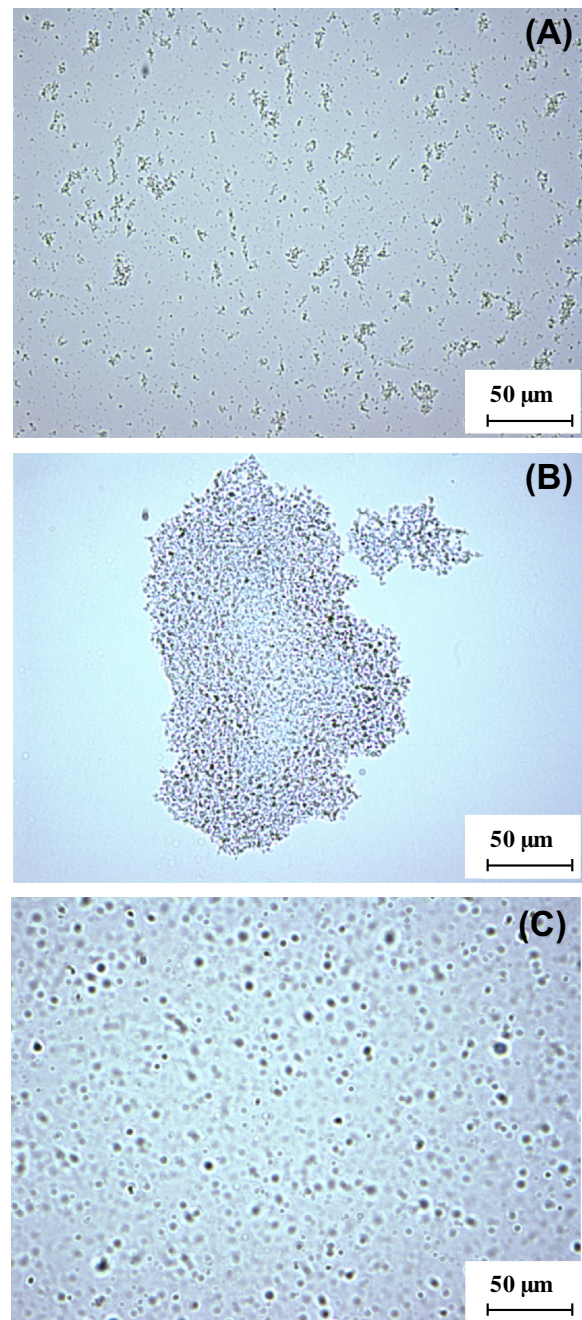
Table 1
D_{43} and span values resulting from the particle size determinations for the $(\beta\text{-lg})_n$ + CMC mixed systems. Measurements conditions: pH 4, temperature 25 °C.

CMC concentration (% wt)	D_{43} (µm)[*]	Span[*]
0	0.29 ± 0.01[a]	1.08 ± 0.03[a]
0.005	14.65 ± 2.04[b]	59.22 ± 2.30[e]
0.01	25.82 ± 2.88[c]	42.56 ± 7.29[d]
0.02	50.79 ± 4.37[d]	2.08 ± 0.05[a,b]
0.04	275.53 ± 24.20[e]	2.27 ± 0.06[a,b]
0.075	198.76 ± 12.20[f]	5.74 ± 0.21[c]
0.15	0.59 ± 0.01[a]	3.23 ± 0.01[b]
0.30	0.73 ± 0.01[a]	2.68 ± 0.09[a,b]

[*] Different letters indicate significant differences ($p < 0.05$).

Fig. 5. Optical microgrpahs of (A) $(\beta\text{-lg})_n$, (B) $(\beta\text{-lg})_n$ + CMC 0.04% wt, and (C) $(\beta\text{-lg})_n$ + CMC 0.3% wt.

As the polysaccharide concentration increases, the link to the most of the negative groups of several polysaccharide molecules to the surface of one aggregate will be favor (Gregory and Barany, 2011). This implies that the CMC molecules in the bulk mixed solution are enough to completely saturate the surface the $(\beta\text{-lg})_n$ constituted a stable suspended system, for instance the core–shell microparticles. The resulting microparticles posses the surface charge of the polysaccharide and keep stable and soluble into the solution bulk as the electrostatic repulsion is favored. Similar behavior was reported for other protein-polysaccharide systems (Güzey et al., 2004; Santipanichwong et al., 2008). It can be concluded that the polyelectrolyte concentration is a parameter of outmost importance, in terms of enhancing the stability of the microparticles suspension for preventing bridging flocculation. As in the particle size distribution profile, higher amounts of CMC (0.3% wt) did not show remarkable variation in D_{43} in comparison to mixed $(\beta\text{-lg})_n$ + CMC systems containing 0.15% (wt) of the polysaccharide.

The span index (Table 1), gives information about the distribution of sizes in the sample, thus the higher the polydispersity the higher the range of distribution of sizes. A first trend could be observed, samples become less homogeneous in terms of size as the CMC bulk concentration increase, for instance 0.02% and 0.04% (wt). Secondly, the polydispersity diminished at higher polysaccharide concentrations. True core–shell microparticles with a low polydispersity were set at CMC concentration higher than 0.15% (wt) in line with the D_{43} variation. Spam index slightly increased for these sample with the polysaccharide amount in comparison with the single $(\beta\text{-lg})_n$, this effect could be attributed to the minimal contribution of some bigger particles in the global distribution.

3.2.2. Microstructure

Optical microscopy, even being relatively simple, resulted a powerful tool to get insight in the spacial arrangement of the

Table 2
D_{43} and span values resulting from the particle size determinations of core–shell microparticles with different CMC concentration, after lyophylization. Measurements conditions: pH 4, temperature 25 °C.

CMC concentration (% wt)	D_{43} (μm)[*]	Span[*]
0.15	264.39 ± 2.70[a]	2.30 ± 0.03[a]
0.30	150.15 ± 21.46[b]	3.95 ± 0.64[b]

[*] Different letters indicate significant differences ($p < 0.05$).

microstructure and the interactions between the structural elements. Fig. 5 displayed such microstructural features. The colorant Coomassie Brillant Blue reacts with high affinity with the protein species staining them in blue. Thus, the $(\beta\text{-lg})_n$ displayed an evenly distributed pattern immersed into a homogeneous background with no visible and segregated domains (Fig. 5A). On the other hand, as the CMC used in the experiments was un-modified, non-labeled, the structures potentially formed by the polysaccharide were not actively visible. $(\beta\text{-lg})_n$ segregated domains, increased gradually in number with the CMC concentration (images not shown). Fig. 5B represents an example of the biggest ones corresponded to those containing 0.04% (wt) of CMC confirming clusters formation by bridging flocculation. A remarkable similarity could be noted between $(\beta\text{-lg})_n$ and $(\beta\text{-lg})_n$ + 0.3% microstructure (Fig. 5C), showing correspondence with the results obtained for D_{43} and the spam trends. A higher number of protein reach domains spatially far apart were detected for the core–shell microparticles, although they seem to be slightly higher in size in the picture, in comparison with $(\beta\text{-lg})_n$ alone.

3.3. Microparticles isolation: lyophilization and rehydration

To determine the effect of lyophilization on the structural integrity of the microparticles, size distribution measurements and
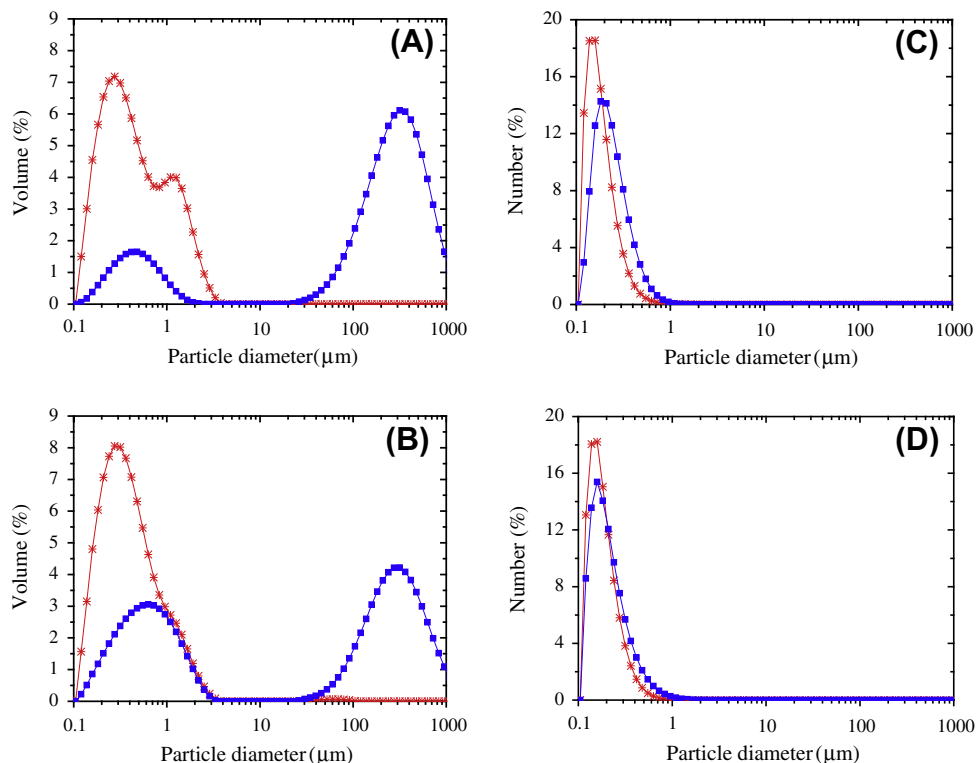
Fig. 6. Volume (A and B) and number (C and D) size distribution of $(\beta\text{-lg})_n$ + CMC ((A and C) 0.15; (B and D) 0.3% wt) (∗) before and (■) after lyophilization. Temperature for SLS measurements 25 °C.

microscopic examination of the freeze-dried and resolubilized samples were performed. The process of freeze–drying of the core–shell microparticles included three steps: freezing of the microparticles suspension, primary drying (sublimation) and secondary drying (desorption). The product was solidified by liquid nitrogen addition, so that the water contained in the material is converted into ice. Freezing is a key step which determines the ice nucleation process and determines the morphology of the frozen materials. Primary drying removes most free water by sublimation, whereas secondary drying gets rid of the bound water and results in low residual water content of the freeze-dried product (Chen et al., 2010).

To restore core–shell particles suspension containing the exact original concentration of microparticles, it was necessary to determine previously the water content in the lyophilized powder. Thus, the moisture determination yields values ranged between 9.00% and 9.64%, d.b. for the $(\beta\text{-lg})_n$ and for $(\beta\text{-lg})_n$ + CMC powders (the variation coefficient for the moisture content data was always lower than 10%). In this way, the mass of water contained in the powder was subtracted from the amount of water added for the microparticles rehydration.

This part of the work includes the data analysis concerning to samples containing the amount of CMC that guaranteed the complete coverage of the $(\beta\text{-lg})_n$ core: 0.15% and 0.3%, wt.

3.3.1. Microparticles size distribution

A potential application of these core–shell microparticles would be the encapsulation of bioactive compounds or drugs and their further delivery, one of the most important factors to reach this aim is the microparticle size (Ye et al., 2010). Fig. 6 shows in a comparatively way the microparticles size distribution before and after lyophilization. First of all, it can be seen that the core–shell systems presented a bimodal volume size distribution after drying (Fig. 6A and B). The maximum peaks values were lower than 1 μm for the first and close to 300 μm for the second one. The smallest particles were dominant when the particle size distribution was analyzed in number (Fig. 6C and D), indicating than the biggest population exerted a limited contribution, for instance only one peak ranging 0.1 and 1 μm was found in the two studied systems.

On the other hand, D_{43}, which can be more influenced for the biggest particles, manifested increased values in comparison with the same sample before being lyophilized. This result would indicate the association of entities after lyophilization and rehydration (Table 2). It could be said that the magnitude of increment was higher at the lowest CMC concentrations. The polydispersity of systems with 0.3% of CMC was slightly increased after the freeze drying process and rehydration (Table 2) in comparison to the span values corresponding to these systems before drying process (Table 1). The particle size and structural features of these systems, i.e. stability of lyophilized core–shell microparticles can be determined by many technological factors, such as freeze-drying protocols and the type of vials or the freeze-dryers. At this respect, Morita et al. (2001) claimed that the degree of condensation during the freezing might complicatedly affect the final sizes and even the morphologies of the isolated particle.

3.3.2. Microstructure of resuspended microparticles

The lyophilized and rehydrated core–shell microparticles were also analyzed by optical microscopy (Fig. 7) with the aimed of comparing the microstructure after the freeze drying. It could be observed that the $(\beta\text{-lg})_n$ (Fig. 7A) did not change radically its general aspect after rehydration in comparison with the $(\beta\text{-lg})_n$ before lyophilization (Fig. 5A). The microstructure turned highly heterogeneous with a great number of protein rich domains where $(\beta\text{-lg})_n$ presented a highly aggregated appearance when the CMC amount was 0.04% (wt) (Fig. 7B), which is in line with the same
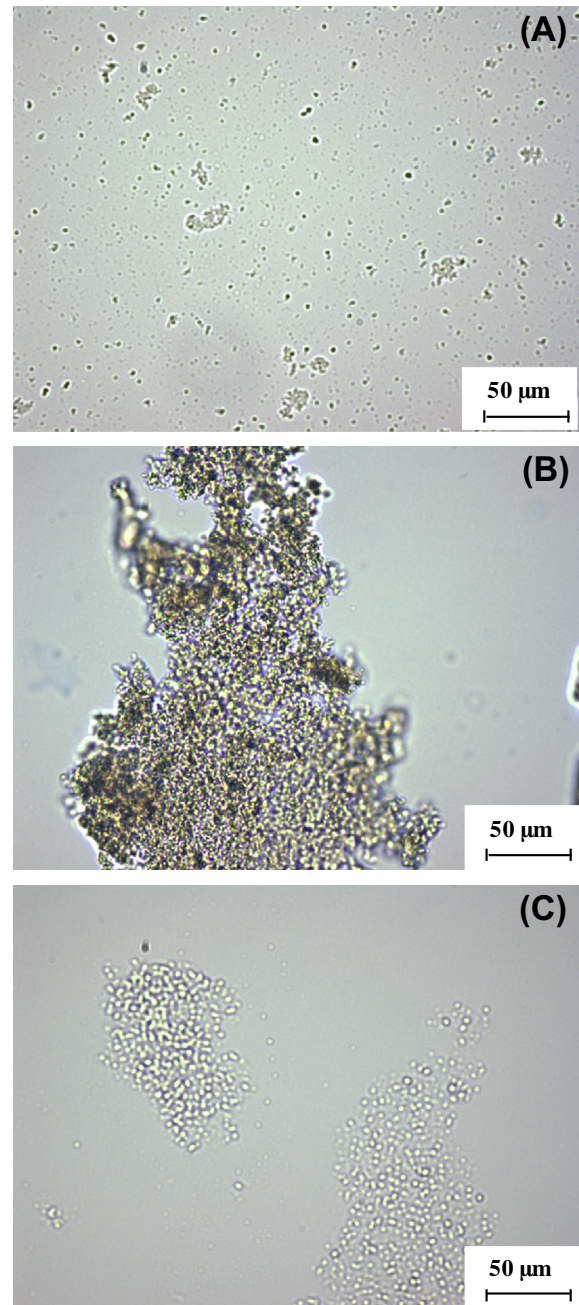

Fig. 7. Optical microgrpahs of (A) $(\beta\text{-lg})_n$, (B) $(\beta\text{-lg})_n$ + CMC 0.04% wt, and (C) $(\beta\text{-lg})_n$ + CMC 0.3% wt, after lyophilization.

sample microstructure previous to be lyophilizated (Fig. 5B). These data are coincident with those from static light scattering (data not shown). Samples with a highest CMC concentration, which in turn had assured the complete $(\beta\text{-lg})_n$ core coverage (0.3% wt), described an heterogeneous system (Fig. 7C) that differ from that before drying (Fig. 5C). Thus, images exhibited loosely bound protein aggregates.

Literature data seems to indicate that there is no a clear trend concerning to the drying process effect on the core–shell systems. Thus, previous works have reported that the possible changes in morphology and microstructure of protein microgels or aggregates structures were induced by the freezing rate. For instance, Shapiro and Cohen (1997) stated that the freezing rate is known to influence alginate gel structure rehydrated easier when freezing
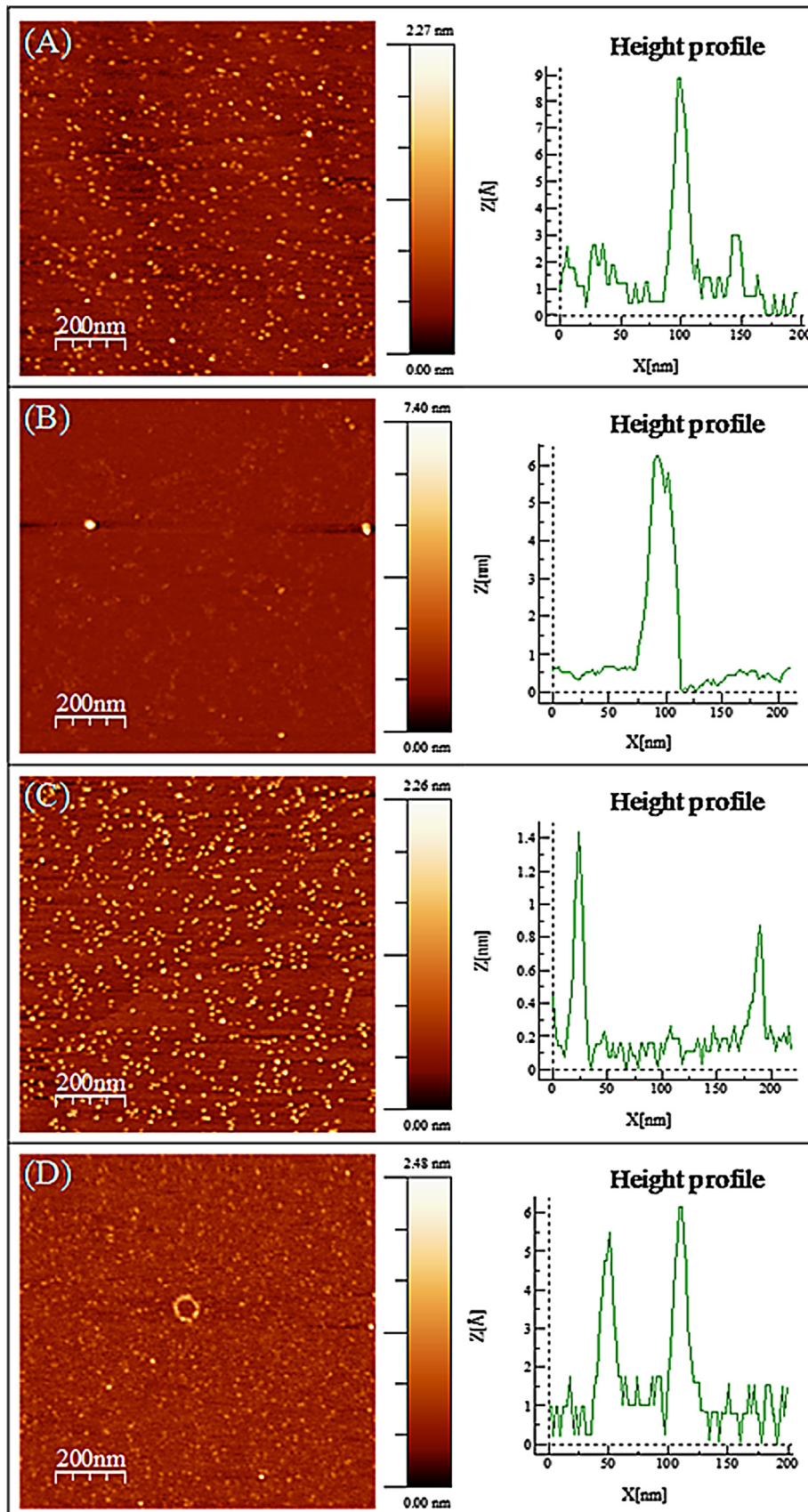
Fig. 8. AFM micrographs illustrating, in the first column, the morphology of (A) $(\beta\text{-lg})_n$, (B) $(\beta\text{-lg})_n$ + CMC 0.04% wt, (C) $(\beta\text{-lg})_n$ + CMC 0.3% wt before lyophilization and (D) $(\beta\text{-lg})_n$ + CMC 0.3% wt after lyophilization. Second column corresponding to samples maximum peak to valley distances and the plots in the third column display their relevant height profiles.

was performed in liquid nitrogen rather than in a freezer. Meanwhile, alginate gel microspheres remained very crumpled after rehydration, whatever the freezing process. On the other hand DeGroot and Neufeld (2001) reported that chitosan-coated alginate beads only partly recover their original diameter after lyophilization and rehydration, rigid membranes possessing less ability to be distorted. More recently, Callewaert et al. (2007) found that the thick of propylene glycol alginate human serum albumin particles shell behaved in the same way and appeared mostly broken when frozen in liquid nitrogen.

3.3.3. Core–shell microparticles appearance: AFM

AFM images are showed in Fig. 8, where the analysis for the considered samples is presented as: the first column show the picture obtained by the AFM technique, the second one shows the length between the maximum and minimum height and the third one describes the height and also the full width taken at half maximum diameter as determined through cross-sectional analysis of a defined part of the image (200 nm). One should keep in mind that the images show microparticles that persisted attached to the mica surface after washing with water pH4 and dried with gaseous nitrogen. The core–shell nanoparticles observed by AFM would correspond to those located in the first part (smaller sizes) of the first peak of Fig. 4. Thus, Fig. 7A, corresponding to the single $(\beta\text{-lg})_n$, describes spherical shapes with an average height of 1 nm. This measure correspond to the height profile of uncovered core, amplified as an average vertical height estimated at about 1 nm, although the maximum peak to valley distance was established to be equal to 2.27 nm, which offered automatically given by the image analysis software.

These features change when the protein core is combined with the different amount of polysaccharide. Thus, Fig. 8B shows bigger particles with an average height of 6 nm, confirming the association of several $(\beta\text{-lg})_n$ probably by the bridging flocculation effect as explained before, being its peak to valley distance of 7.40 nm. Fig. 8C, corresponding to microparticles constituted by $(\beta\text{-lg})_n$ + CMC 0.3%, wt, manifested a reduction for these parameters up to 1.5 nm for average height and a maximum distance for peak to valley equal to 2.14, which practically identical to that of the protein core (Fig. 8A). AFM imaging confirmed the complete core surface coverage by 0.3% of CMC.

Lyophilizated core–shell particles (Fig. 8D) described general topography similar to that before drying. The height profile and peak to valley distance slightly increased. It can be said that from the AFM results, it not resulted evident that the freeze drying process of the core shell systems and their further rehydration had a relevant effect on the morphology observed at the nanoscale. The width for the isolated microparticles seemed to be slightly increase as can be observed in the "x" axe of the high profile graph corresponding to this sample.

4. Conclusions

Core–shell type microparticles could be designed and characterized in terms of their structure. The optimal mass concentration between the protein core and the CMC for stable core–shell microstructure formation could be determined, i.e. the polysaccharide bulk concentration that assured the complete surface protein core. The amount of the polysaccharide kept direct relation with the particles size.

Firstly, the electrochemical and aggregation properties for the core construction were studied. The union between the protein core, of a controlled size, and the polyelectrolyte was verified. As such an interaction was pH dependent, it was favoured when both species presented opposite electrical charge. This fact keep technological

consequences as $(\beta\text{-lg})_n$ + CMC core–shell microparticles could be used in foods whose pH falls between the protein core pI and the polysaccharide pK_a. More specifically, these microparticles could find application into food technology as fat replacers and/or encapsulating agent for different substances exerting controlled release. The "world of acid foods" is wide; some examples are dairy products, fruit juices, dressings and desserts.

On the other hand, $(\beta\text{-lg})_n$ + CMC microparticles could successfully isolated as a powder. The results obtained for the D_{43} values and optical microscopy indicated some kind of aggregation after lyophilization which can be minimal considering the particle size distribution expressed in number. Meanwhile, the AFM results did not evidence that such aggregation was extensive. The lyophilization process applied to the microparticles isolation deserves more insight in order to minimize the effects of aggregation, even it effect on the microparticles size and morphology was limited, it could be improved. Finally, the electrostatic deposition proved to be a useful strategy for generate microparticles with a $(\beta\text{-lg})_n$ core and a carboxymethylcellulose shell.

Acknowledgements

References

Aberkane, L., Jasniewski, J., Gaiani, C., Hussain, R., Scher, J., Sanchez, C., 2012. Structuration mechanism of β-lactoglobulin – acacia gum assemblies in presence of quercetin. Food Hydrocolloids 29, 9–20.

Akkerman, C., Van Der Goot, A.J., Venema, P., Gruppen, H., Vereijken, J.M., Van Der Linden, E., Boom, R.M., 2007. Micrometer-sized fibrillar protein aggregates from soy glicinin and soy protein isolates. J. Agric. Food Chem. 55, 9877–9882.

Anarjan, N., Tan, C.P., 2013. Developing a three component stabilizer system for producing astaxanthin nanodispersions. Food Hydrocolloids 30 (1), 437–447.

Arzeni, C., Pérez, O.E., Pilosof, A.M.R., 2012. Functionality of egg white proteins as affected by high intensity ultrasound. Food Hydrocolloids 29 (2), 308–316.

Aymard, P., Nicolai, T., Durand, D., Clark, A., 1999. Static and dynamic scattering of β-lactoglobulin aggregates formed after heat-induced denaturation at pH 2. Macromolecules 32 (8), 2542–2552.

Berne, B.J., Pecora, R., 1976. Dynamic Light Scattering with Applications to Chemistry, Biology and Physics. Wiley-Interscience, New York.

Broersen, K., Van Teeffelen, A.M.M., Vries, A., Voragen, A.G.J., Hamer, R.J., De Jongh, H.J.J., 2006. Do sulfhydryl groups affect aggregation and gelation properties of ovalbumin? J. Agric. Food Chem. 54 (14), 5166–5174.

Bromley, E.H.C., Krebs, M.R.H., Donald, A.M., 2005. Aggregation across the length-scales in β-lactoglobulin. Faraday Discuss. 128, 13–27.

Callewaert, M., Laurent-Maquin, D., Edwards-Lévy, F., 2007. Albumin-alginate-coated microspheres: resistance to steam sterilization and to lyophilization. Int. J. Pharm. 344 (344), 161–164.

Chanasattru, W., Jones, O.G., Decker, E.A., McClements, D.J., 2009. Impact of cosolvents on formation and porperties of biopolymer nanoparticles formed by heat treatment of β-lactoglobulin–pectin complexes. Food Hydrocolloids 23, 2450–2457.

Chen, L.Y., Remondetto, G.E., Subirade, M., 2006. Food protein-based material as nutraceutical delivery systems. Trend Food Sci. Technol. 17 (5), 272–283.

Chen, C., Han, D., Cai, C., Tang, X., 2010. An overview of liposome lyophilization and its future potential. J. Controlled Release 142, 299–311.

Coviello, T., Matricardi, P., Marianecci, C., Alhaique, F., 2007. Polysaccharide hydrogels for modified release formulations. J. Controlled Release 119 (1), 5–24.

Dalgleish, D.G., 1990. The conformations of proteins on solid/water interfaces – caseins and phosvitin on polystyrene latices. Colloids Surf. 46 (2), 141–155.

DeGroot, A.R., Neufeld, R.J., 2001. Encapsulation of urease in alginate beads and protection from α-chymotrypsin with chitosan membranes. Enzyme Microb. Technol. 29 (6–7), 321–327.

Elzoghby, A.O., Abo El-Fotoh, W.S., Elgindy, N.A., 2011. Casein-based formulations as promising controlled release drug delivery systems. J. Controlled Release 153 (3), 206–216.

Emerich, D.F., Thanos, C.G., 2007. Targeted nanoparticles-based drug delivery and diagnosis. J. Drug Target. 15 (3), 163–183.

European Union Commission, 1996. Commission Directive 96/77/EC.

Galazka, V.B., Dickinson, E., Ledward, D.A., 1996. Effect of high pressure on the emulsifying behaviour of β-lactoglobulin. Food Hydrocolloids 10 (2), 213–219.

Goldberg, M., Langer, R., Jia, X.Q., 2007. Nanostructured materials for applications in drug delivery and tissue engineering. J. Biomater. Sci. – Polym. Ed. 18 (3), 241–268.

Gregory, J., Barany, S., 2011. Adsorption and flocculation by polymers and polymer mixtures. Adv. Colloid Interface Sci. 169 (1), 1–12.

Gu, Y.S., Decker, A.E., McClements, D.J., 2005. Production and characterization of oil-in-water emulsions containing droplets stabilized by multilayer membranes consisting of β-lactoglobulin, ι-carrageenan and gelatin. Langmuir 21 (13), 5752–5760.

Güzey, D., Kim, H.J., McClements, D.J., 2004. Factors influencing the production of o/w emulsions stabilized by β-lactoglobulin–pectin membranes. Food Hydrocolloids 18 (6), 967–975.

Hansen, P.M., Hidaldo, J., Gould, I.A., 1971. Reclamation of whey protein with carboxymethylcellulose. J. Dairy Sci. 54, 830–834.

Harnsilawat, T., Pongsawatmanit, R., McClements, D.J., 2006. Characterization of β-lactoglobulin–sodium alginate interactions in aqueous solutions: a calorimetry, light scattering, electrophoretic mobility and solubility study. Food Hydrocolloids 20, 577–585.

Heinze, T., Liebert, T., 2001. Unconventional methods in cellulose functionalization. Prog. Polym. Sci. 26, 1689–1762.

Ho, Q.T., Carmeliet, J., Datta, A.K., Defraeye, T., Delele, M.A., Herremans, E., Opara, L., Ramon, H., Tijskens, E., van der Sman, R., Van Liedekerke, P., Verboven, P., Nicolai, B.M., 2013. Multiscale modeling in food engineering. J. Food Eng. 114 (3), 279–291.

Hoffmann, M.A.M., van Mil, P.J.J.M., 1999. Heat induced aggregation of β-lactoglobulin as a function of pH. J. Agric. Food Chem. 47, 1898–1905.

Huang, X., Kakuda, Y., Cui, W., 2001. Hydrocolloids in emulsions: particle size distribution and the interfacial activity. Food Hydrocolloids 15, 533–542.

Hunter, R.J., 2001. Foundations of Colloid Science. Oxford Clarendon Press.

Ilgin, P., Avci, G., Silan, C., Ekici, S., Aktas, N., Ayyala, R.S., John, V.T., Sahiner, N., 2011. Colloidal drug carries from (sub)micron hyaluronic acid hydrogel particles with tunable properties for biomedical applications. Carbohydr. Polym. 82 (3), 997–1003.

ISO 6731. 1989. Milk, Cream and Evaporated Milk-Determination of Total Solids Content (Reference Method). ISO, Geneva, Switzerland.

Jones, O.G., McClements, D.J., 2011. Recent progress in biopolymer nanoparticle and microparticle formation by heat-treating electrostatic protein-polysaccharide complexes. Adv. Colloid Interface Sci. 167 (1–2), 49–62.

Kulkarni, G.T., Gowthamarajan, K., Dhobe, R.R., Yohanan, F., Surech, B., 2005. Development of controlled release spheroids using natural polysaccharide as release modifier. Drug Delivery 12 (4), 201–206.

Lakkis, J.M., Thies, C., 2007. Microencapsulation of flavors by complex coacervation. In: Lakkis, J.M. (Ed.), Encapsulation and Controlled Release Technologies in Food Systems. Blackwell Publishing Ltd, Oxford, UK, pp. 148–170.

Lavaggi, M.L., Cabrera, M., Aravena, M.A., Olea-Azar, C., López de Ceráin, A., Monge, A., Pachón, G., Cascante, M., Bruno, A.M., Pietrasanta, L.I., González, M., Cerecetto, H., 2010. Study of benzo[a]phenazine 7,12-dioxide as selective hypoxic cytotoxin-scaffold. Identification of aerobic-antitumoral activity through DNA fragmentation. Bioorg. Med. Chem. 18, 4440–4443.

Laville, M., Babin, J., Londono, I., Legros, M., Nouvel, C., Durand, A., Vanderesse, R., Leonard, M., Six, J.-L., 2013. Polysaccharide-covered nanoparticles with improved shell stability using click-chemistry strategies. Carbohydr. Polym. 93 (1), 537–546.

Lee, H.S., Choi, J.I., Kim, J.H., Lee, K.W., Chung, Y.J., Shin, M.H., Byun, M.W., Shin, M.G., Lee, J.W., 2009. Investigation on radiation degradation of carboxymethylcellulose by ionizing irradiation. Appl. Radiat. Isot. 67, 1513–1515.

Leroux, J., Langendorff, V., Schick, G., Vaishnav, V., Mazoyer, J., 2003. Emulsion stabilizing properties of pectin. Food Hydrocolloids 17 (4), 455–462.

Lesmes, U., McClements, D.J., 2012. Controlling lipid digestibility: response of lipid droplets coated by β-lactoglobulin-dextran Maillard conjugates to simulated gastrointestinal conditions. Food Hydrocolloids 26, 221–230.

Malvern-Instruments. Calculating volume distributions from dynamic light scattering data. <http://www.malvern.com>.

Mandal, B., Bhattacharjee, H., Mittal, N., Sah, H., Balabathula, P., Thoma, L.A., Wood, G.C., 2013. Core–shell-type lipid–polymer hybrid nanoparticles as a drug delivery platform. Nanomed.: Nanotechnol. Biol. Med. 9, 474–491.

Mehalebi, S., Nicolai, T., Durand, D., 2008. Light scattering study of heat-denatured globular protein aggregates. Int. J. Biol. Macromol. 43, 129–135.

Mirabedini, S.M., Dutil, I., Farnood, R.R., 2012. Preparation and characterization of ethyl cellulose-based core shell microcapsules containing plant oils. Colloids Surf., A 394, 74–84.

Morita, T., Horikiri, Y., Suzuki, T., Yoshino, H., 2001. Preparation of gelatin microparticles by co-lyophilization with poly(ethylene glycol): characterization and application to entrapment into biodegradable microspheres. Int. J. Pharm. 219 (219), 127–137.

Murúa-Pagola, B., Beristain-Guevara, C.I., Martínez-Bustos, F., 2009. Preparation of starch derivatives using reactive extrusion and evaluation of modified starches as shell materials for encapsulation of flavoring agents by spray drying. J. Food Eng. 91 (3), 380–386.

Navarra, G., Leone, M., Militello, V., 2007. Thermal aggregation of β-lactoglobulin in presence of metal ions. Biophys. Chem. 31, 52–61.

Santipanichwong, R., Suphantharika, M., Weiss, J., McClements, D.J., 2008. Core-shell biopolymer nanoparticles produced by electrostatic deposition of beet pectin onto heat-denatured β-lactoglobulin aggregates. J. Food Sci. 73 (6), 23–30.

Schokker, E.P., Singh, H., Pinder, D.N., Norris, G.E., Creamer, L.K., 1999. Characterization of intermediates formed during heat-induced aggregation of β-lactoglobulin AB at neutral pH. Int. Dairy J. 9, 791–800.

Schokker, E.P., Singh, H., Creamer, L.K., 2000. Heat-induced aggregation of β-lactoglobulin A and B with α-lactalbumin. Int. Dairy J. 10, 843–853.

Shapiro, L., Cohen, S., 1997. Novel alginate sponges for cell culture and transplantation. Biomaterials 18 (8), 583–590.

Sharma, M., Haque, Z.U., Wilson, W.W., 1996. Association tendency of β-lctoglobulin AB purified by gel permeation chromatography as determined by dynamic light scattering under quiescent conditions. Food Hydrocolloids 10, 323–328.

Su, J., Huang, Z., Yuan, X.-Y., Wang, X.-Y., Li, M., 2010. Structure and properties of carboxymethyl cellulose/soy protein isolate blend edible films crosslinked by Maillard reactions. Carbohydr. Polym. 79, 149–153.

Surroca, Y., Haverkamp, J., Heck, A.J.R., 2002. Towards the understanding of molecular mechanisms in the early stages of heat-induced aggregation of β-lactoglobulin AB. J. Chromatogr. A 970, 275–285.

Turgeon, S.L., Beaulieu, M., Schmitt, C., Sanchez, C., 2003. Protein–polysaccharide interactions: phase-ordering kinetics, thermodynamic and structural aspects. Curr. Opin. Colloid Interface Sci. 8 (4–5), 401–414.

Ubbink, J., Kruger, J., 2006. Physical approaches for the delivery of active ingredients in foods. Curr. Opin. Colloid Interface Sci. 17 (2), 244–254.

Vásconez, M.B., Flores, S.K., Campos, C.A., Alvarado, J., Gerschenson, L.N., 2009. Antimicrobial activity and phisical properties of chitosan-tapioca starch based edible films and coatings. Food Res. Int. 42 (7), 762–769.

Verheul, M., Roefs, S.P.F.M., de Kruif, K.G., 1998. Kinetics of heat-induced aggregation of β-lactoglobulin. J. Agric. Food Chem. 46, 896–903.

Wu, J., Kong, T., Yeung, K.W.K., Shum, H.C., Cheung, K.M.C., Wang, L., To, M.K.T., 2013. Fabrication and characterization of monodisperse PLGA-alginate core-shell microspheres with monodisperse size and homogeneous shells for controlled drug release. Acta Biomater. 9 (7), 7410–7419.

Ye, M., Kim, S., Park, K., 2010. Issues in long-term protein delivery using biodegradable microparticles. J. Controlled Release 146 (2), 241–260.